Study on a new mooring system integrating catenary with taut mooring

Chun-Yan Ji, Zhi-Ming Yuan

Abstract: The merits and demerits of catenary mooring system and taut mooring system, which are commonly used nowadays, are analyzed. Falling somewhere between these two systems, a new mooring system integrating catenary with taut mooring is proposed. In order to expound and prove the advantages of this new system, the motion performance of a semi-submersible platform is simulated by employing full time domain coupled analysis method. Comparing the result of new mooring system with that of taut mooring system, it can be concluded that the movement of the platform using the new type mooring system is smaller than that using the taut mooring system, which ensures a better working conditions. Furthermore, the new mooring system is also compatible with the characteristic of catenary mooring system, which eliminates the requirement of anti-uplift capacity of the anchors.

Key words: catenary; taut mooring system; semi-submersible platform; lumped mass; coupled analysis

1 Introduction

As shallow water hydrocarbon reserves continue to reduce in contrast to ever increasing global demand, recent years have seen an increasing use of floating production systems in deep-water sites, with water depths in the region of 1000–3000m being of special interest. Meanwhile, traditional catenary mooring system has presented many drawbacks as water depth increases (Schmidt et al. 2006; Nuno Fonseca, 2009). Firstly, catenary chain or wire relies heavily on their own weight, which can provide restoring forces. As a result, it will not only increase production costs, but also heighten line tensions at the fairlead and enlarge vertical load on the vessel when the line is lifted from the sea bottom (Johanning et al., 2007). This growth in vertical load can be important as it effectively decreases the vessel useful payload. Secondly, the length of catenary chain can be quite large, which may bring an increase in mooring radius and consequently raise the risk of collision between mooring lines and other undersea equipment. Besides, since the restoring forces provided by catenary chain are not adequate to keep a small

platform offsets, drilling condition will deteriorate. Due to these drawbacks, a taut mooring system, which adopts synthetic polymeric ropes, has been increasingly used in the last 15 years, as shown by various studies (Arcandra Tahar, 2008; API RP 2SM, 2001; Hooker, 2000; Pearson, 2002; Petruska et al., 2005), which highlight the potential of using synthetic fibers in the naval industry, mainly for deep water (off-shore) mooring. For one thing, synthetic polymeric ropes can provide great restoring forces through their axial stiffness. To a large extend, it can reduce mean- and low-frequency platform offsets and improve the drilling condition (Chakrabartis, 2005). For another, synthetic fiber lines are considerably lighter, very flexible and can absorb imposed dynamic motions through extension without causing an excessive dynamic tension (Liu Hai-xiao and Huang Ze-wei, 2007).

However, there are still some disadvantages in using synthetics, such as more complicated and not as well understood as the traditional rope. This leads to over-conservative designs that strip them of some of their advantages (Chakrabartis, 2005). Furthermore, there is an included angle (usually 30-45deg.) between taut lines and seafloor (You Ji-kun and Wang Yan-ying, 2009). And thus, anchor point will be subject to a vertical component of tension, which requires the use of anchors designed to allow uplift at the seabed. These include suction anchors that demand complicated technology in anchor design and installation. Nevertheless, the advantage of catenary mooring system can be a complement. Owing to the gravity, there is a long tangency between lines and sea bed, which guarantees a tension without vertical component.

Considering the merits and demerits of catenary mooring system and taut mooring system, a new mooring system integrating catenary with taut mooring is proposed in this paper. Based on polyester taut mooring, some lumped masses are applied to the end of mooring lines at fixed intervals, which can form a catenary end, tangent to the seabed. In this way, suction anchors are not needed since anchor point only suffers horizontal tension. To illustrate the validity of this new system, a semi-submersible platform located in Gulf of Mexico is simulated by SESAM software. Numerical results including motion responses of 6 DOF, effective tension of lines and the shape of catenary end are presented in this paper. Finally, these results of new system are also compared with that of traditional taut mooring system.

2 Design proposal

Fig.1 and Fig.2 show the traditional taut mooring system and the new taut mooring system with catenary end respectively.

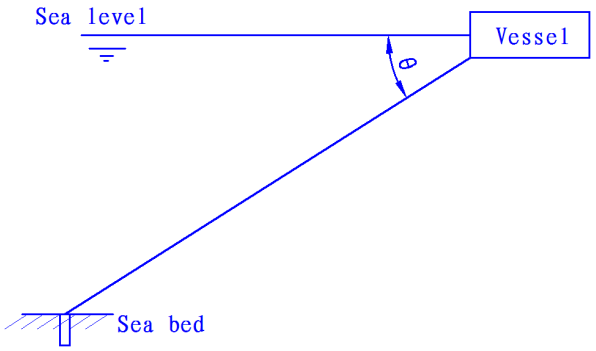

Fig.1 Original taut mooring line

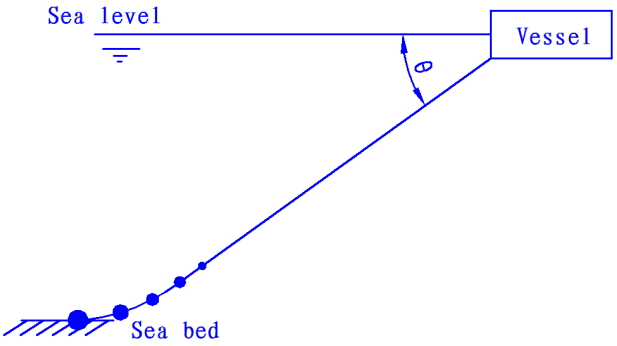

Fig.2 New mooring line

Fig.1 shows the original taut mooring line is tightened almost as a straight line and the line end is fixed by suction anchor. The angle between the line and the sea level is θ and the tension at the end of line is totally provided by the anchor. Fig.4 shows that there is a little difference between the traditional taut mooring line and the new mooring line in the aspects of line length and mooring radius. In spite of this, the latter scheme requires several lumped masses in the catenary end at uniform intervals. The weight of masses diminishes gradually from the bottom. Thus, the end of lines will perform as a catenary. When they are subject to maximum tension, it should be designed to satisfy that the lumped mass next to anchor point will not leave sea bed. In this way, tangent can be guaranteed and there is no vertical component of tension at anchor point since it is counteracted by a natural weight. When the tension decreases, masses will be supported by the sea floor, thereby alleviating the tension at fairlead as well as increasing the vessel's useful payload capacity.

3 Equations of motion

The motion equation of the coupled system in the time domain can be written as (Low and Langley, 2006)

$$\begin{bmatrix} \mathbf{M}_V & 0 \\ 0 & \mathbf{M}_L \end{bmatrix} \begin{bmatrix} \ddot{\mathbf{x}}_V(t) \\ \ddot{\mathbf{x}}_L(t) \end{bmatrix} + \begin{bmatrix} \mathbf{C}_V & 0 \\ 0 & 0 \end{bmatrix} \begin{bmatrix} \dot{\mathbf{x}}_V(t) \\ \dot{\mathbf{x}}_L(t) \end{bmatrix} + \begin{bmatrix} \mathbf{K}_V & 0 \\ 0 & 0 \end{bmatrix} \begin{bmatrix} \mathbf{x}_V(t) \\ \mathbf{x}_L(t) \end{bmatrix} = \begin{bmatrix} \mathbf{F}_V(t) \\ \mathbf{F}_L(t) \end{bmatrix} \tag{1}$$

where $\mathbf{x}(t)$ is the displacement vector, **M, C, K** are the mass, damping and stiffness matrices of

the coupled system respectively. $\mathbf{M}_V$ contains the structural mass and the added mass of the vessel. $\mathbf{C}_V$ contains the damping on the vessel from viscous skin drag, wave drift damping and radiation damping. The added mass and radiation (potential) damping matrices of the vessel can be obtained from a radiation analysis. These are in general frequency dependent; in the time domain they can either be Fourier transformed to give the retardation functions of the vessel, or treated more approximately by using fixed values chosen at a representative frequency. $\mathbf{F}$ is the external force vector; V and L represent the vessel and the lines respectively. $\mathbf{K}_V$ is the linear hydrostatic stiffness matrix of the vessel. There are no contributions to the damping and stiffness matrices from the lines since these effects are included as external forces on the RHS of Eq. (1) for the purpose of time integration. External forces on the vessel can be composed of wave, current and wind part. The wave forces acting on a floating vessel are well documented in the literature, and thus only a brief outline of the key results is given here. A linear diffraction analysis provides the vector of first order transfer functions $\mathbf{T}^{(1)}$, defined so that in a regular wave of frequency

$$\mathbf{F}^{(1)}(\omega) = \mathbf{T}^{(1)}(\omega)\eta(\omega) \tag{2}$$

where $\mathbf{F}^{(1)}$ is the vector of first order forces and η is the wave amplitude. For time domain simulations of a random sea state, the first order forces can be expressed as a sum over constituent sea state components, and this sum can be evaluated efficiently by using the Fast Fourier Transform technique to yield a time history of the forces (Newland, 1984).

In addition to the first order forces, the vessel is subjected to second order forces arising from nonlinear hydrodynamic effects. These forces are determined from a second order diffraction analysis, and only the slowly varying forces caused by difference frequencies in the surge, sway and yaw are pertinent to the present study. The vector of slow drift quadratic transfer functions (QTFs) $\mathbf{T}^{(2)}$ is defined from the interaction between a pair of waves with frequencies ω_n and ω_m, and is defined so that

$$\mathbf{F}^{(2)}(\omega_m, \omega_n) = \mathbf{T}^{(2)}(\omega_m, \omega_n)\eta(\omega_m)\eta(\omega_n) \tag{3}$$

where $\mathbf{F}^{(2)}$ is the vector of second order forces, $\eta(\omega_m)$ and $\eta(\omega_n)$ are two wave amplitudes. For time domain analysis the time history of the second order wave forces in a random sea state can

be expressed as a double summation over the first order wave components that comprise the sea state; this expression may be evaluated using the efficient method described by Langley (1986). For frequency domain analysis, the cross-spectra matrix of the second order forces $S_{FF}^{(2)}$ is needed, and this is given by (Langley, 1987)

$$S_{FF}^{(2)}(\omega) = 8\int_0^{\infty} \mathbf{T}^{(2)}(\mu, \omega+\mu)\left[\mathbf{T}^{(2)}(\mu, \omega+\mu)\right]^{H} \times S_{\eta\eta}(\mu) S_{\eta\eta}(\omega+\mu) d\mu \tag{4}$$

where $S_{\eta\eta}$ is the wave spectrum and the subscript H denotes the Hermitian transpose. Each diagonal component of $S_{FF}^{(2)}$ is real and is consistent with the form of the second order force spectrum given by Pinkster (1979).

The wind force is calculated based on the instantaneous wind and body velocities. The force is calculated according to the following formula (DNV Software, 2008):

$$\mathbf{F}_w = C_j(\alpha) v^2 \tag{5}$$

where j is the degree of freedom, C is the wind force coefficient for the instantaneous relative direction, v is the relative velocity between body and wind, α is the direction relative velocity in local coordinate system. Optionally, the velocity of the body may be omitted when calculating relative velocity.

All body current forces are computed using the current velocity at the surface (z–0). Traditionally, the viscous hull surge and sway force and yaw moment have been calculated based on current coefficients and the instantaneous magnitude of the translational relative velocity between the vessel and the fluid. The current drag forces are then expressed by (DNV Software, 2008):

$$q_{CU}^{(k)}(\alpha, t) = C_1^{(k)}(\alpha)|u(t)| + C_2^{(k)}(\alpha)|u(t)|^2 \tag{6}$$

$$|u|^2 = (v_1 - \dot{x}_1)^2 + (v_2 - \dot{x}_2)^2 \tag{7}$$

$$\alpha = \arctan\frac{v_2 - \dot{x}_2}{v_1 - \dot{x}_1} \tag{8}$$

where k is the degree of freedom, C_1 is the linear current force coefficient, C_2 is the quadratic current force coefficient, u is the relative velocity between low-frequency body velocity and current velocity, α is the relative angle between direction of low-frequency body velocity and current velocity, v_1, v_2 is the current velocity components in the surface for floating bodies and at the center of gravity for submerged bodies, $\dot{x}$ is the vessel velocity components in the vessel

coordinate system.

4 Numerical study

4.1 Description of semi-submersible platform

A typical semi-submersible (as shown in Fig.3) in Gulf of Mexico with the water depth of 913.5 m is used as a numerical example to illustrate the effectiveness of the new type mooring system. The essential characteristics of the vessel are summarized in Table 1.

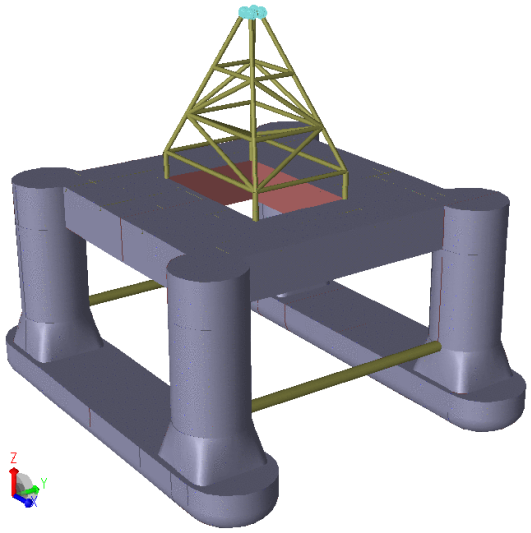

Fig.3 The structure model of the semi-submersible

Tab.1 Essential characteristics of the platform

Length	Width	Draft	Water depth	Displacement
80m	80m	20m	913.5m	25000t

4.2 Design of the new mooring system

(1) Description of the mooring lines

To fully compare the mooring effect of the new mooring system with that of traditional taut mooring system, the same arrangement of mooring lines is adopted, as shown in Fig.4. There are 12 combined mooring lines with chain, wire and chain, as illustrated by Z.M. Yuan et al. (2010). The schematic plot of the arrangement for mooring lines is shown in Fig.4 and Tab.2 shows the main particulars of mooring lines.

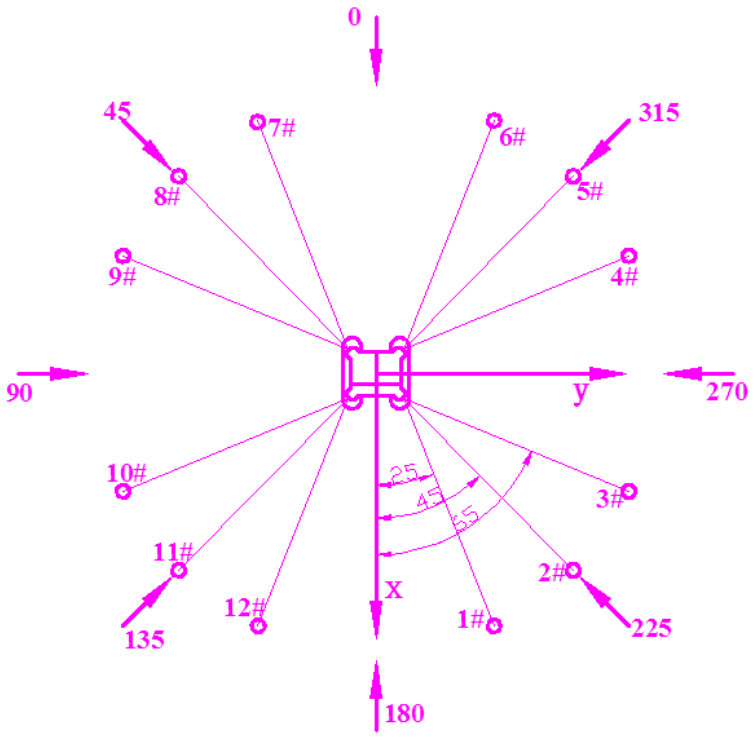

Fig.4 Arrangement of the mooring lines

Tab.2 Main particulars of the mooring lines

Segment	L (m)	P(KN)	D (m)	W(t/m)	EA(MN)	C_{dn}/C_{dt}	C_{in}/C_{it}	MBL(KN)
Chain	152	2233	0.098	0.192	802	2.45/0.65	2/0.5	8927
Polyester	1440	2233	0.178	0.007	300	1.2/0.3	1.15/0.2	9786
Chain	141	2233	0.098	0.192	802	2.45/0.65	2/0.5	8927

The symbols appeared in Fig.4 are defined as follows: L is the length of segment, P is the pretension, D represents diameter, EA represents stiffness, C_{dn} and C_{dt} are the normal and tangent drag coefficients, C_{in} and C_{it} represent normal and tangent added inertia coefficient, MBL is the mean breaking load.

(2) Arrangement of lumped masses

Based on the same arrangement of mooring lines, the concept of new mooring system is brought forward, which applies the lumped masses to the line end. There are 5 lumped masses arranging at the terminal 100m of the line. The length between two masses is 20m, as shown in Fig.4, where m_1=20t, m_2=15t, m_3=10t, m_4=5t, m_5=2t.

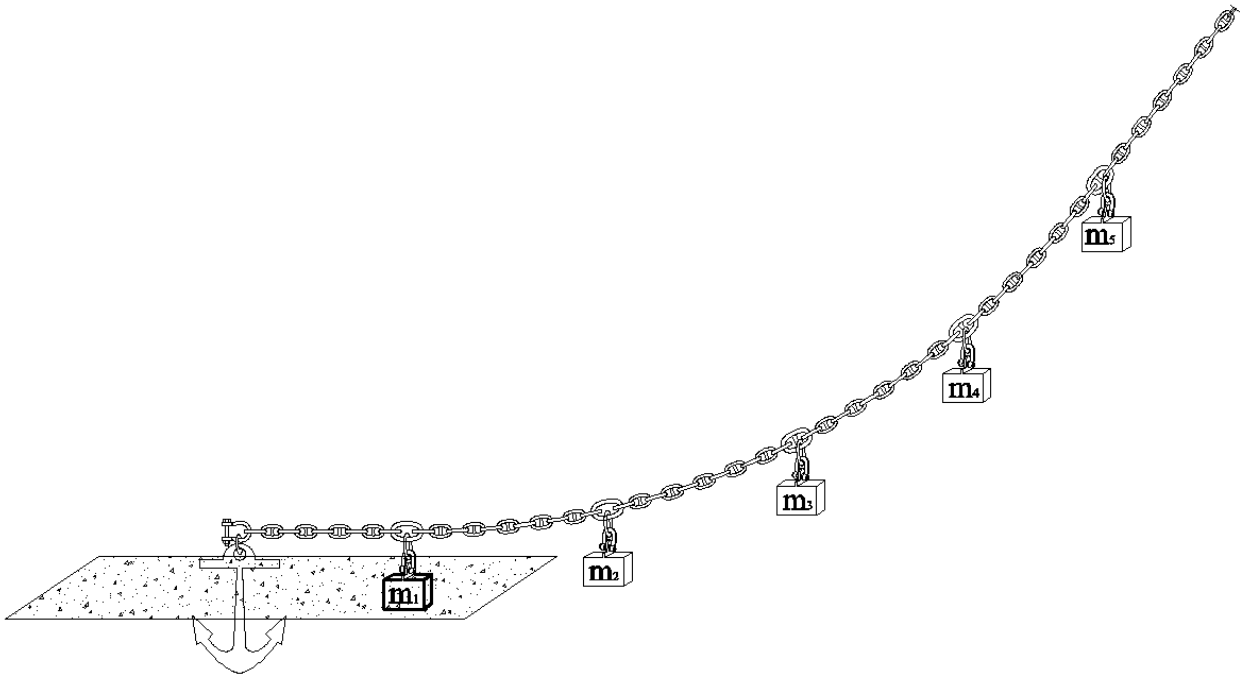

Fig.4 Arrangement of lumped masses

(3) Environmental Data

The 100-year extreme hurricane condition at the GOM is used, which is one of the severest in the world. The wave condition is represented with the significant wave height of 12.19 m, the peak period of 14 sec, and the overshooting parameter of 2.5. The wind spectrum given by API formulae is used as the design condition. The mean one hour sustained wind velocity at the reference height of 10 m is 41.12 m/s. The current is mainly induced by the storm. The velocity of current at the sea surface is 1.0668 m/s, and it remains at this value down to 60.96 m under the sea surface. From 60.96 m to 91.44 m under the sea surface, the current speed varies from 1.0668 m/s to 0.05 m/s. For the intermediate region between 60.96 m to 91.44 m, the current profile is determined by the linear interpolation. The current speed is kept uniform at 0.05 m/s from 91.44 m under the surface to the sea bottom. The wave, wind and current approach the vessel at angles of 90°, 210°and 150 ° (measured counterclockwise from the x-axis) respectively.

4.3 Comparison analysis on the new mooring system and the original taut mooring system

(1) Motion responses of the vessel

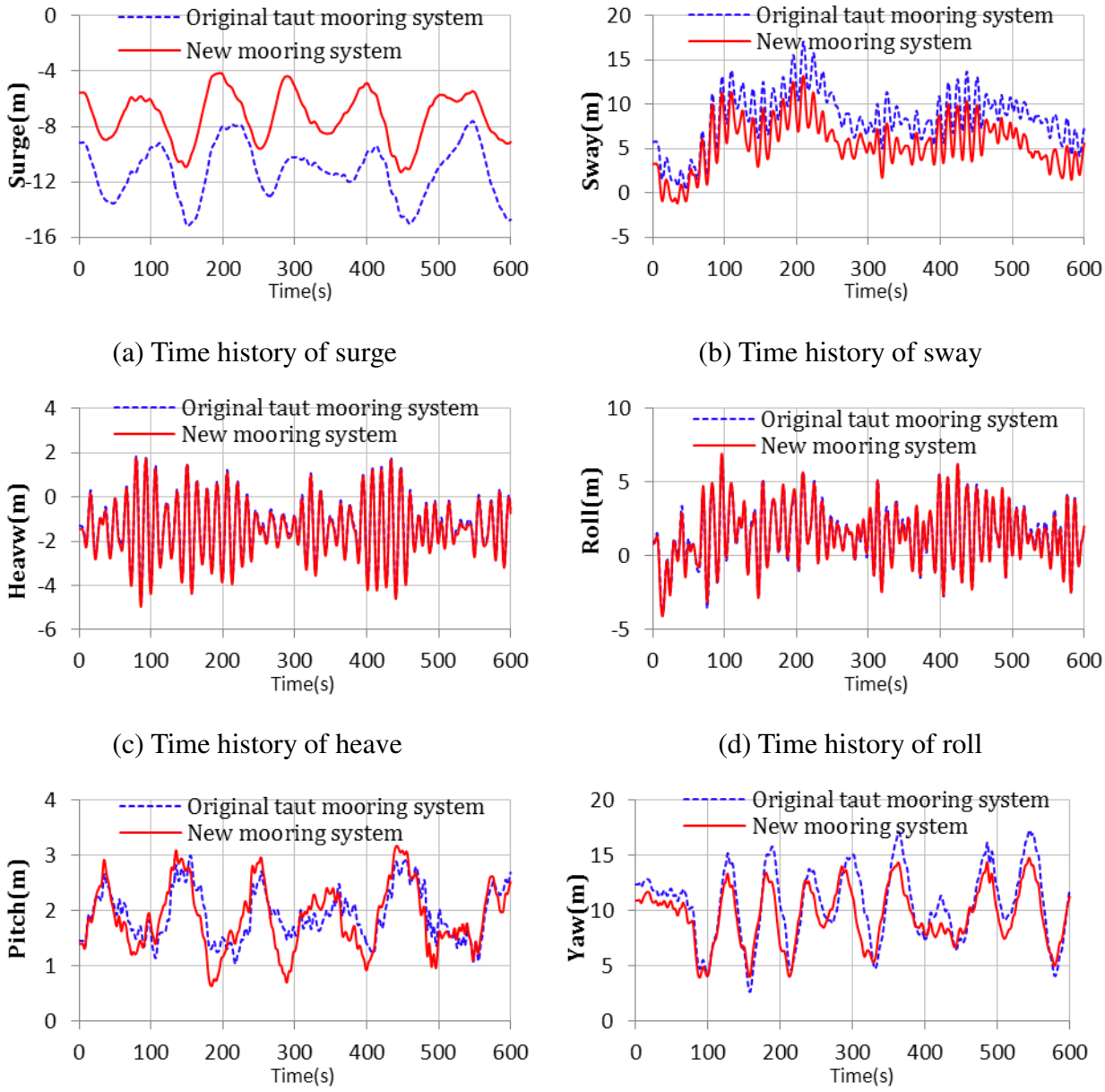

(a) Time history of surge

(b) Time history of sway

(c) Time history of heave

(d) Time history of roll

(e) Time history of pitch

(f) Time history of yaw

Fig.5 Time history of the motion

Fig.5 shows the simulation results of vessel motion. From figs.5 (a), (b) and (f), it can be seen when it refers to horizontal-plane motions (surge, sway, yaw), the motion performance of vessel can be improved if the new mooring system is employed. And the motion response amplitude becomes lower in comparison with that of the original taut mooring system under the same conditions. When it comes to heave and roll, there is almost no difference between these two mooring systems. But, the response amplitude of pitch is slightly higher when the new mooring system is used. Fig.6 shows the trajectory path of vessel in horizontal-plane, where the

origin of coordinates is defined to the center of gravity. Fig.7 shows the time history of displacement.

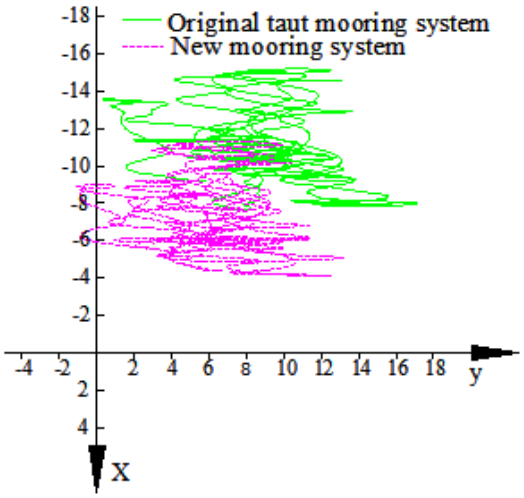

Fig.6 Trajectory path of vessel in horizontal-plane

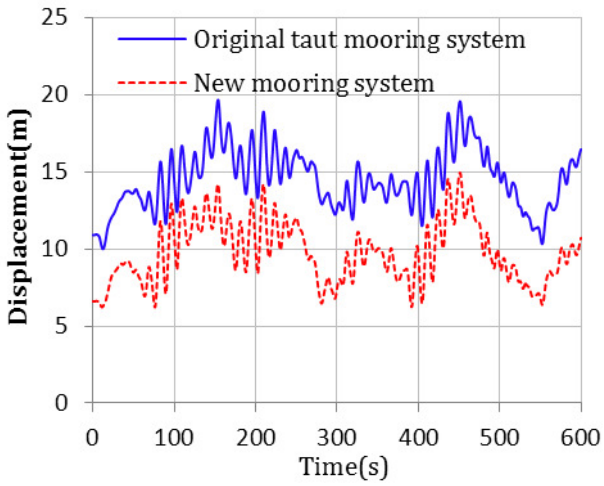

Fig.7 Time history of displacement

From Fig.6, it is clearly seen that the motion radius of vessel in the horizontal-plane is much lower when the new mooring system is used. In addition, vessel displacement also decreases (as shown in Fig.7). And the reduction of maximum value of displacement can reach 24%. The simulation results of the new mooring system and the original taut mooring system are displayed in Tab.3.

Tab.3 Result of motion (unit: m, deg.)

	Original taut mooring system			New mooring system			Reduction
	Mean	RMS	Max	Mean	RMS	Max	of Max (%)
Surge(m)	-11.22	1.92	15.17	-7.28	1.79	11.3	25.5%
Roll(deg)	1.48	1.86	6.8	1.42	1.88	6.93	-1.9%
Sway(m)	8.43	3.13	17.08	5.58	2.77	13.19	22.8%
Pitch(deg)	1.93	0.46	3	1.89	0.6	3.17	-5.7%
Heave(m)	-1.32	1.25	4.75	-1.45	1.26	4.96	-4.4%
Yaw(deg)	10.6	3.3	17.29	9.59	2.62	14.78	14.5%
Displacement(m)	14.5	1.95	19.66	9.74	1.97	14.94	24.0%

To study the motion response from spectrum view, the results in the time domain is transferred by taking the Fourier transform.

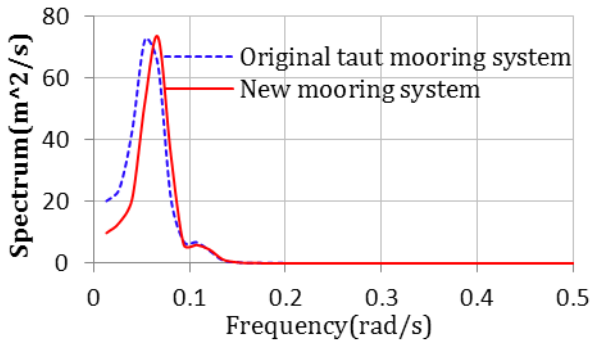

(a) Spectrum of surge

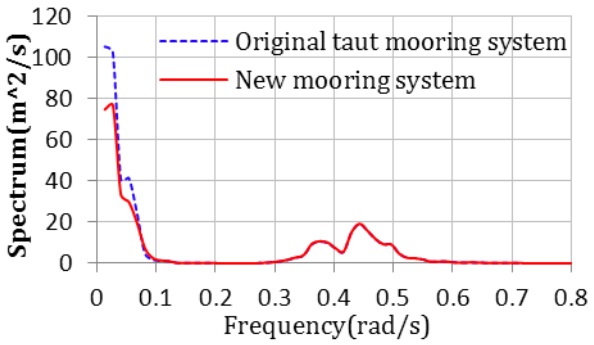

(b) Spectrum of sway

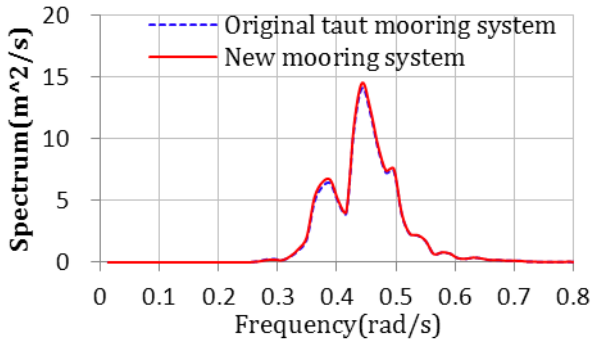

(c) Spectrum of heave

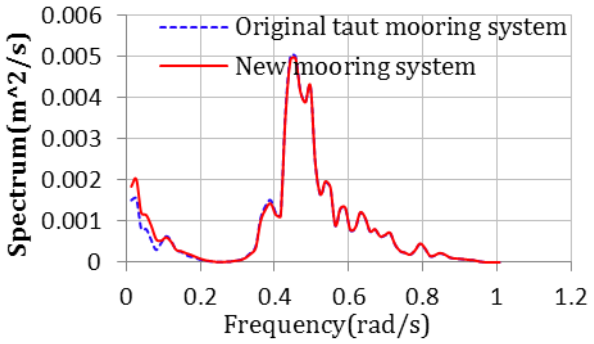

(d) Spectrum of roll

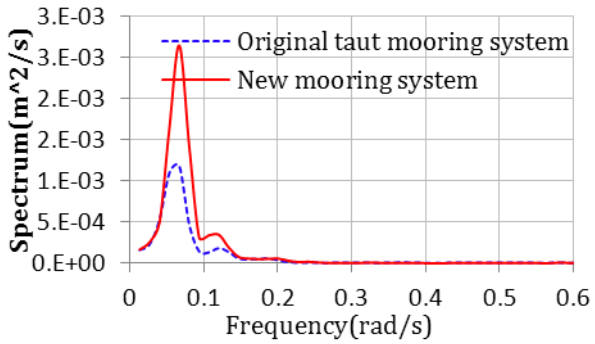

(e) Spectrum of pitch

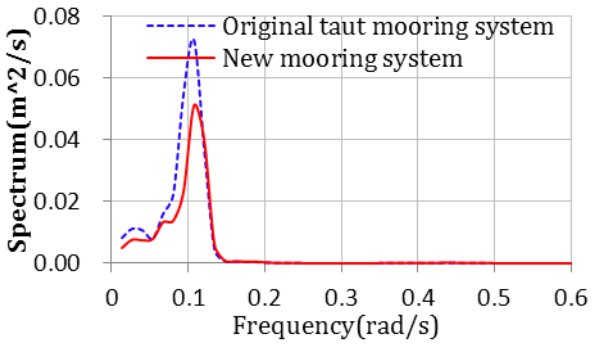

(f) Spectrum of yaw

Fig.8 The spectrum of the motion

The dynamic response in a random sea is hereon at two timescales: the wave frequency response (WF) at the wave frequency (0.2–2rad/s) and the low frequency (LF) response at the in-plane resonances (0-0.2rad/s). These two types of motion are coupled via the geometric nonlinearity of the mooring lines and the nonlinear drag forces acting on the lines. Any dynamic analysis must therefore account simultaneously for both types of motion. From Fig.8, it can be drawn that all the motion responses in WF range maintain the same value, while visible distinction only occurs in LF range. Fig.8 (a) indicates that in surge motion, the peak value of

spectrum of the new mooring system keeps almost the same with that of the original taut mooring system. But the spectral peak frequency of the new mooring system suffers a little increase. Figs.8 (b) and (f) illustrates that in sway and yaw motion, the spectral peak value decrease significantly when the new mooring system is adopted. On the contrary, Fig.8 (b) shows an increase in spectral peak value of the new mooring system in pitch motion. However, since the pitch motion is not fierce (the maximum value of which is only 3deg), a small increase in response amplitude will not add great influence to vessel motion. When it comes to heave and roll, as shown in Figs.8 (c) and (d), the new mooring system and the original taut mooring system share accordant responses in the entire frequency range. It can also been drawn from Fig.8 that the low frequency (LF) responses play dominate roles in surge, sway, pitch and yaw, while in heave and roll, WF responses are more visible.

(2) Responses of mooring lines

The results above illustrate that the new mooring system can greatly improve the motion responses of the vessel. But, line tension is another major factor which determines the rationality of mooring line arrangement. On the account of the direction of the environmental loads, the lines are subject to uneven loads. Effective tension of Line 10 is in a direction away from the platform offsets, which renders Line 10 be subject to the largest tension. Therefore, Line 10 is selected to be the analysis object in this paper. Fig.9 displays the static tension distribution along the longitudinal length of Line10 of the new mooring system and the original taut mooring system.

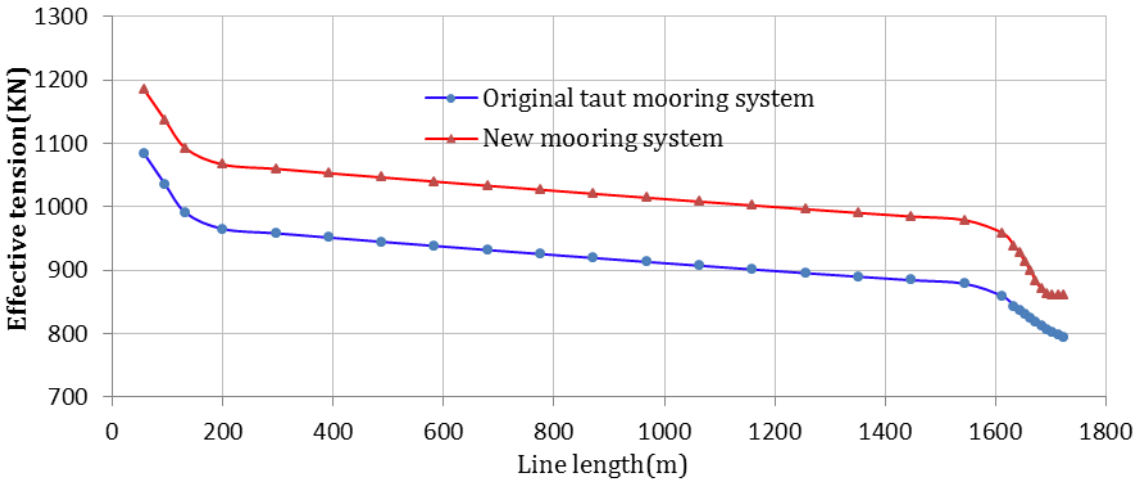

Fig.9 Static tension

Fig.9 shows that effective tension diminishes as the line extends to the sea bed and it arrives

to its peak at fairlead. Since the segments between 0 to 152m and 1592 to 1733m are chain, the rate of descent is more significant than that of the polyester segment. And the new mooring system adds to this downward trend. But the last few elements of the new mooring lines keep the same tension, which indicates these elements are lying on the sea bed. Besides, in comparison with the original taut mooring system, static tension increases after the application of the new mooring system because of the mass gravity. Fig.10 shows the simulation results of dynamic tension at the fairlead of Line 10 under the two mooring systems.

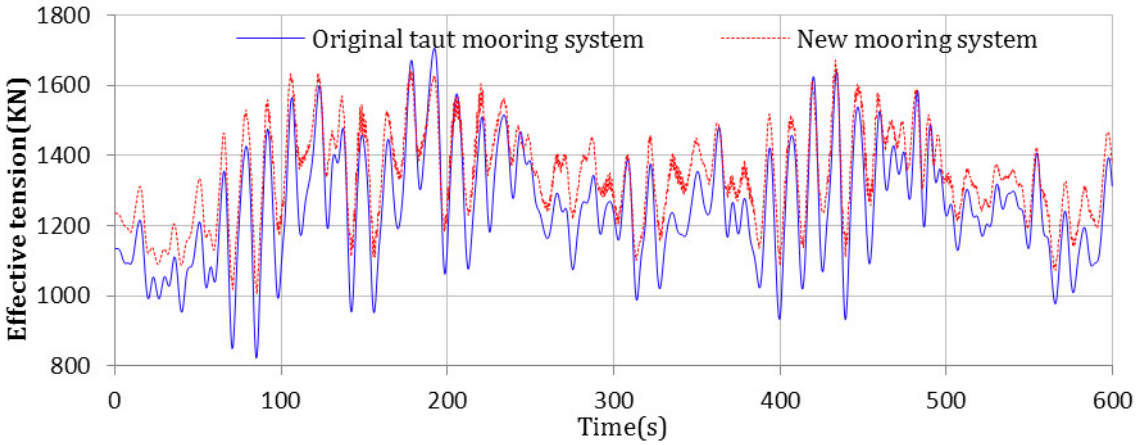

Fig.10 Dynamic tension

Fig.10 reveals that although static line tension of the new mooring system experiences a visible increase as compared with that of the original taut mooring system, the peak of transient response has been buffered by 2.1% as well as RMS, which witnesses a reduction by 18.2%.

Except the peak period of the wave mentioned above (14s), another two period cases (12s and 16s) are simulated. The results of different periods are shown in Tab.4.

Tab.4 Dynamic tension results of different peak period of the wave

Peak Period(s)	New mooring system			Original taut mooring system		
	Max(kN)	Mean(kN)	RMS(kN)	Max(kN)	Mean(kN)	RMS(kN)
12s	1638.64	1317.47	104.22	1653.71	1224.48	116.59
14s	1672.1	1343.12	129.5	1706.68	1253.81	159.22
16s	1669.2	1344.71	136.19	1750.58	1268.76	177.62

In addition to the original water depth of 913.5m, another two cases (500m and 750m) are also simulated. The results of different water depths are shown in Tab.5.

Tab.5 Dynamic tension results of different water depths

Water depth	New mooring system	Original taut mooring system

(s)	Max(kN)	Mean(kN)	RMS(kN)	Max(kN)	Mean(kN)	RMS(kN)
500m	1766	1327	156	2140	1217	254
750m	1666	1331	118	1637	1242	134
913.5m	1742	1371	138	1836	1264	191

From the results of Tabs.4 and 5, it can be concluded that duo to the lumped masses arranged at the end of the new taut mooring system, the mean tension of the lines is increased. However, the maximal value and RMS of the new mooring system are lower than that of original taut mooring system, which illustrates that the new mooring system will decrease the tension fluctuation and acquire a reasonable tension distribution and subdued tension peak. And thus, the breaking risk of the lines can be cut down.

(3) Discussion of the distribution of the lumped mass

Mass arrangements at the line end play an important role in the new mooring system design since they will significantly affect the catenary shape at the line end. This shape mainly lies on altitude value of each node. Meanwhile, the direction of tension at anchor point is dominated by the angle between the lines and sea bed. Since element length at the line end is 20m, which equals the length between $\mathbf{m_1}$ and the anchor point, this elevation angle is only rested with the altitude value of $\mathbf{m}_1$. Furthermore, the biggest elevation angle will appear at Line10 since it is subject to the maximum tension. Tab.5 presents three different arrangements of the lumped masses. Figs.11-13 shows the time history of altitude value of these three schemes. Fig.14 gives the results without the lumped masses.

Tab.4 Arrangement of lumped masses (unit: t)

	m_1	m_2	m_3	m_4	m_5
Scheme Ⅰ	10	8	6	4	2
Scheme Ⅱ	20	15	10	5	2
SchemeⅢ	30	25	20	15	10

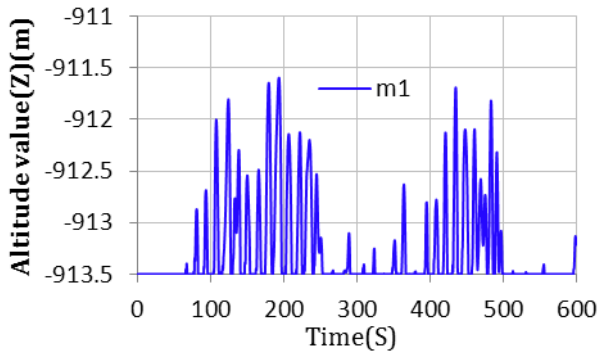

(a) Altitude value of Scheme Ⅰ

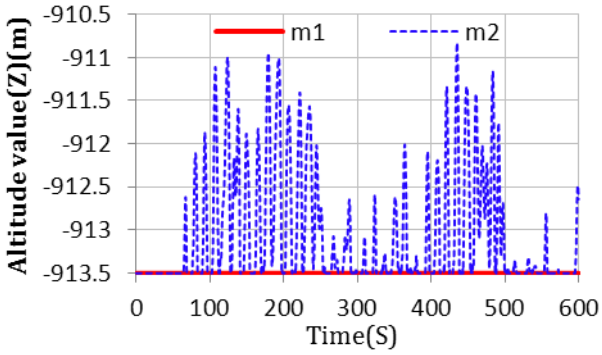

(b) Altitude value of Scheme Ⅱ

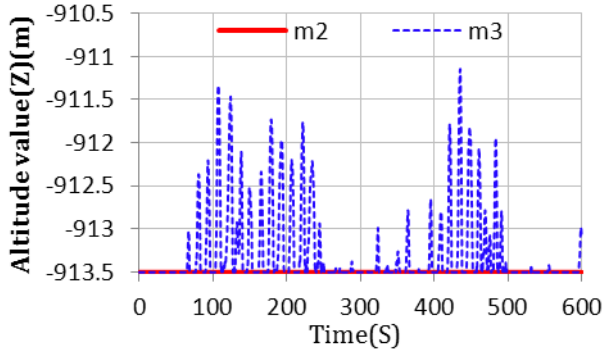

(c) Altitude value of SchemeⅢ

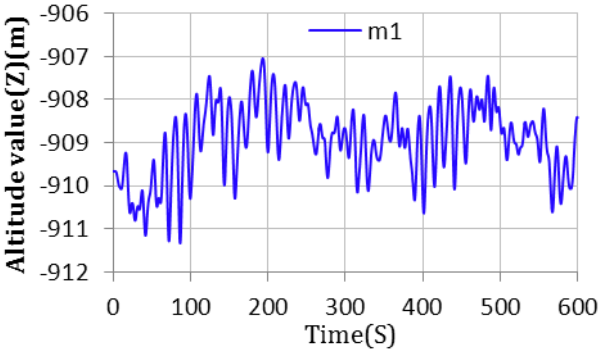

(d) Altitude value without masses

Fig.11 Altitude value of different schemes

From Fig.11 (a), it can be drawn that in Scheme Ⅰ, the altitude value of $\mathbf{m_1}$ varies with the time. When the altitude value is -913.5m, equaling to that of water depth, it illustrates $\mathbf{m_1}$ is lying on the sea bed. But when the altitude value stays above -913.5m, it indicates $\mathbf{m_1}$ is lifted by the tension. Therefore, Scheme Ⅰ is not the ideal distribution since it cannot keep the tangent to the sea bed all the time. It can be seen from Fig.11(b) that in Scheme Ⅱ, the altitude value of $\mathbf{m_1}$ stays in -913.5m all along, which indicates the elevation angle equals zero even though the tension reaches its peak. Meanwhile, the altitude value of $\mathbf{m_2}$ may sometimes exceed -913.5. In contrast with two schemes hereinbefore, in SchemeⅢ, $\mathbf{m_1}$ and $\mathbf{m_2}$ are all supported by the sea bed all along while $\mathbf{m_3}$ experiences a little fluctuations. Although it can guarantee the tangent, this scheme works too conservative. Fig.11 (d) indicates that the altitude value without masses is more significant than that of other schemes. When the tension peak of Line 10 occurs, the catenary shape can be attained after linking altitude value of each node located in the last 141m chain segment, as shown in Fig.12.

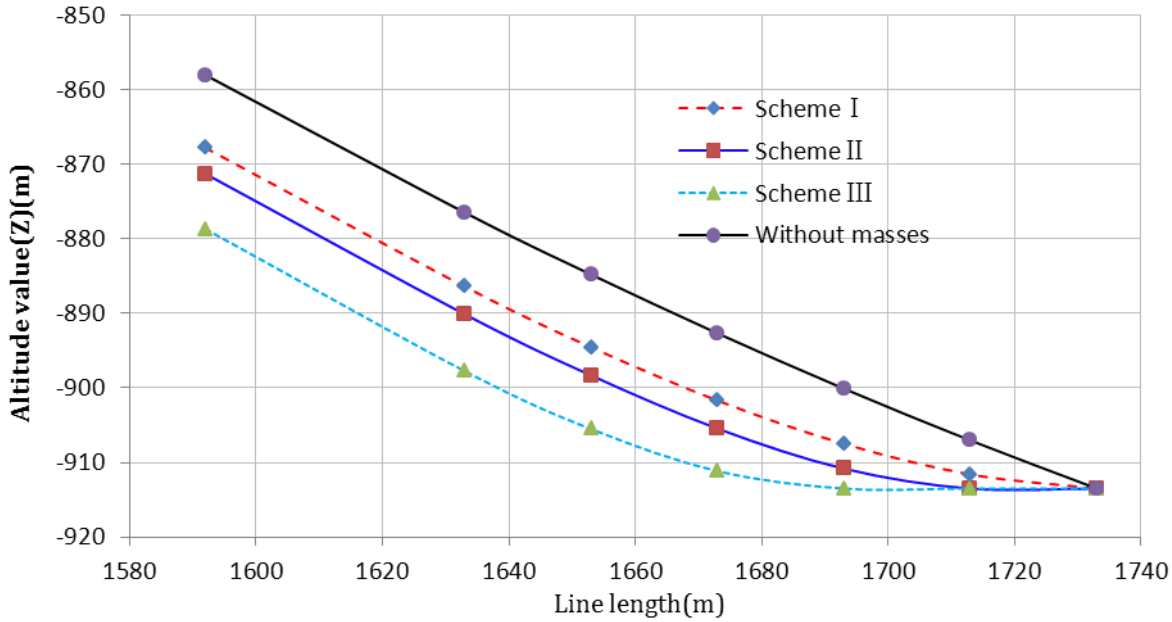

Fig.12 Shapes of the catenary end

It can be clearly seen from Fig.12 that when the original taut mooring system is used, the change in curvature is not obvious and the elevation angle may stay in a biggish level. Thus, anchor point will be subject to a vertical component of tension. But if masses arrangement of Scheme Ⅱ is applied, a catenary end will form to keep anchor point from vertical loads.

5 Conclusions

Based on the advantages of catenary mooring system and taut mooring system, a new mooring system integrating catenary with taut mooring is proposed. Numerical simulation of the new mooring system in different water depths has been carried out. By comparing simulation results obtained with new mooring system to those obtained with the traditional taut mooring system, the following conclusions can be reached:

1) The new mooring system integrating catenary with taut mooring can improve the motion performance of the vessel. The new mooring system will bring improvements to the low frequency (LF) response of the vessel. In this way, the motion of the vessel can be decreased, which will improve the working conditions on the vessel.
2) The tension peak of the lines can be reduced by this new mooring system integrating catenary with taut mooring. Although the static tension may increase under the weight of masses, the peak value and the fluctuating range will decrease, which can reduce the

breaking risk of the lines.

3) The new mooring system integrating catenary with taut mooring can keep the anchor from vertical loads. A reasonable arrangement of the masses may form a catenary at line end, which will eliminate the requirement of anti-uplift capacity of the anchors.

In summary, the new mooring system integrating the catenary lines with the taut lines proposed in the paper has a better performance compared to the traditional taut mooring system. However, the new mooring system's performance has only been demonstrated through the numerical simulations. Further studies based on experimental investigation are needed to verify the results and the feasibility of the construction process for the new mooring system needs also to be assessed.

References

API RP 2SM 2001. Recommended Practice for Design, Analysis, and Testing of Synthetic Fiber Ropes in Offshore Technology Conference, OTC 10779, Houston, Texas.

Arcandra Tahar, M.H. Kim. Coupled-dynamic analysis of floating structures with polyester mooring lines [J]. Ocean engineering, 35(2008), 1676-1685.

D. Petruska, J. Geyer, R. Macon, M. Craig, A. Ran, N. Schulz, Polyester mooring for the mad dog spar-design issues and other considerations [J], Ocean Eng. 32 (7) (2005) 767.

J.G. Hooker. Synthetic Fiber Ropes for Ultra-deep Water Moorings in Drilling and Production Applications, Technical Paper Marlow Ropes, OMT Singapore, 2000.

Johanning, L., Smith, G.H., Wolfram, J. Measurements of static and dynamic mooring line damping and their importance for floating WEC devices [J]. Ocean Engineering, 34:14-15, 1918-1934.

Langley RS. On the time domain simulation of second order wave forces and induced responses. Appl Ocean Res 1986;8(3):134–43.

Langley RS. Second order frequency domain analysis of moored vessels. Appl Ocean Res 1987;9(1):7–18.

Liu Hai-xiao, Huang Ze-wei. A New Type Deep-Water Mooring System and Numerical Analytical Techniques [J].Ocean Technology, 2007, 26(2):6-10.

N.J. Pearson, Experimental Snap Loading of Synthetic Fiber Ropes, Doctoral Thesis, Virginia Polytechnic Institute and State University, Blacksburg, 2002.

Newland DE. An introduction to random vibrations and spectral analysis.2nd ed. Longman; 1984.

Nuno Fonseca, Ricardo Pascoal, Tiago Morais, Renato Dias. Design of a mooring system with synthetic ropes for the FLOW wave energy converter. OMAE2009-80223, Honolulu, Hawaii, 2009.

Pinkster JA. Mean and low frequency wave drifting forces on floating structures. Ocean Eng 1979;6(6):593–615.

S. Chakrabartis. Handbook of offshore engineering [M]. Vol.8. Amsterdam: Elsevier, 2005.

SIMO - Theory Manual Version 3.6, rev: 1, DNV Software, 2008.

T.M. Schmidt, C. Bianchini, M.M.C. Forte, S.C. Amico, A. Voronoff, R.C.F. Gonc-alves. Socketing of polyester fibre ropes with epoxy resins for deep-water mooring applications [J]. Polymer Testing , 25 (2006) 1044–1051.

You Ji-kun, Wang Yan-ying. Designing Investigation of the Taut-Wire Mooring Systems for Deepwater Semi-submersible Platforms [J]. China Offshore Platform, 2009, 24(1):24-30.

Y.M.Low, R.S.Langley. Time and frequency domain coupled analysis of deep-water floating production systems [J].Applied Ocean Research, 2006, (28).371-385.

Yuan-zhiming, Ji-chunyan, Chen-minglu. Full time domain coupled analysis of semi-submersible platform. Ocean Technology, 2010(04), 81-87.